arXiv:1002.1474v1 [physics.atom-ph] 7 Feb 2010

Evaluation of the screened QED corrections to the g factor and the hyperfine splitting of lithiumlike ions

D. A. Glazov,[1,2] A. V. Volotka,[1,2] V. M. Shabaev,[1] I. I. Tupitsyn,[1] and G. Plunien[2]

[1] *Department of Physics, St. Petersburg State University, Oulianovskaya 1, Petrodvorets, St. Petersburg 198504, Russia*

[2] *Institut für Theoretische Physik, Technische Universität Dresden, Mommsenstraße 13, D-01062 Dresden, Germany*

Abstract

The screened QED corrections of the first orders in α and $1/Z$ to the g factor and the hyperfine splitting of lithiumlike ions are evaluated within *ab initio* quantum electrodynamical approach. The complete gauge-invariant set of the two-electron self-energy diagrams in the presence of the magnetic field and a dominant part of the two-electron vacuum-polarization diagrams are calculated. The most accurate values of the g factor of Li-like lead and uranium are presented. The theoretical prediction for the specific difference of the hyperfine splittings of H- and Li-like bismuth is improved.

PACS numbers: 12.20.Ds, 31.30.Jv, 31.30.Gs

I. INTRODUCTION

The bound-electron g factor has been the subject of intense experimental and theoretical investigations over the past decade. Recent measurements for low-Z hydrogenlike ions with a spinless nucleus have reached the precision of 10^{-9} [1–3]. Together with the corresponding theoretical studies these experiments have lead to the new value of the electron mass, four times more accurate than the previously accepted value (see Ref. [4] and references therein). Experimental investigations of ions with more than one electron are anticipated in the nearest future. In particular, measurements of the g factor of H-like and Li-like calcium and silicon are currently in progress by the Mainz-GSI collaboration [5]. An extension of these studies to high-Z H-like, Li-like, and B-like systems planned in the framework of the HITRAP project [6, 7] will provide a stringent test of the bound-state QED in the strong electric field of the nucleus. Moreover, investigations of the g factor of heavy B-like ions can lead to an independent determination of the fine structure constant [8]. The motivation for studying the g factor of Li-like and B-like ions follows from the higher theoretical accuracy that can be reached for a specific difference of the g factor values of H-like and Li-like ions (or H-like and B-like ions) of the same isotope. Various effects on the g factor of H-like ions were investigated during the last two decades: one-loop [9–16] and two-loop [17, 18] QED corrections, recoil corrections [19–21], nuclear polarization effect [22], and nuclear size effect [23]. The theoretical investigations of the g factor of Li-like ions were conducted in Refs. [24–27]. Apart from the one-electron contributions to the g factor of $2s$ state, the effects of the interelectronic interaction should be taken into account in three-electron ions. The one-photon exchange correction was evaluated in the framework of QED in Ref. [25]. The higher-order contributions of the interelectronic interaction were calculated by means of the large-scale configuration-interaction Dirac-Fock-Sturm method in Ref. [26]. Still, the uncertainty associated with these contributions amounts to more than half of the total theoretical uncertainty. The effect of the interelectronic interaction on the QED corrections was treated within two approaches. For low-Z ions the perturbation theory to the leading orders in αZ was employed [24, 26]. For middle-Z and high-Z ions more accurate results were obtained by evaluating the one-electron QED corrections in an effective screening potential [27]. Nevertheless, for all values of Z the uncertainty of the screened QED effects contributes significantly to the total uncertainty, and the rigorous evaluation of these effects is in demand.

Hyperfine structure of highly charged ions comprises another sensitive tool for probing QED

effects in strong fields. Accurate measurements of the ground-state hyperfine splittings were performed for several H-like ions, including ^{209}Bi, ^{165}Ho, ^{185}Re, ^{187}Re, ^{207}Pb, ^{203}Tl, and ^{205}Tl in Refs. [28–32]. These experiments motivated corresponding theoretical investigations [33–40]. The theoretical uncertainty of the hyperfine splitting is also dominated by the nuclear effects, mainly by the Bohr-Weisskopf effect [35]. The theoretical investigations have shown [40] that simultaneous studies of the hyperfine splitting in H-like and Li-like ions of the same isotope can significantly improve the accuracy of the theoretical prediction. As a result, the ground-state hyperfine splitting in Li-like bismuth was predicted to a high accuracy using the experimental result for the $1s$ hyperfine splitting in H-like bismuth [38–40]. The indirect measurement of the hyperfine splitting of lithiumlike bismuth performed in Livermore yielded value of 820(26) meV [41]. Determination of this splitting to a much higher accuracy (of about 10^{-7}) is planned at GSI in the framework of the HITRAP project [42]. This requires further improvements of the theoretical predictions for Li-like ions and, in particular, evaluations of the QED screening effect. An approximate treatment of this effect was accomplished in Refs. [39, 43–47] by employing an effective screening potential in calculations of the one-loop self-energy and vacuum-polarization diagrams.

Rigorous evaluation of the two-electron self-energy and vacuum-polarization diagrams (Figs. 1 and 2) remained a challenge for theory until recently. In our Letter [48] the complete αZ-dependent contributions of the two-electron self-energy diagrams and a dominant part of the two-electron vacuum-polarization diagrams have been evaluated for the hyperfine structure of Li-like bismuth and for the g factor of Li-like lead. In the present paper we describe in detail the evaluation of the screened quantum electrodynamical correction in presence of external magnetic field. Furthermore, we extend our calculations to the wide range of nuclear charge $Z = 20 - 83$ in case of the hyperfine splitting. The accuracy of the theoretical prediction for the specific difference of the hyperfine splittings of H- and Li-like bismuth is improved. As to the g factor, we present the results for lead and uranium ions.

The relativistic units ($\hbar = 1, c = 1, m = 1$) and the Heaviside charge unit [$\alpha = e^2/(4\pi), e < 0$] are used throughout the paper.

II. FORMULATION

A systematic derivation of the QED corrections in a fully relativistic approach requires the use of perturbation theory starting with a one-electron approximation, described by the Dirac equation,

$$[-i\boldsymbol{\alpha}\cdot\boldsymbol{\nabla}+\beta m+V(\mathbf{x})]\,\psi_n(\mathbf{x})=\varepsilon_n\psi_n(\mathbf{x})\,. \tag{1}$$

In our present treatment the binding potential $V(\mathbf{x})=V(|\mathbf{x}|)$ denotes the nuclear potential only. The interaction of the electrons with the quantized electromagnetic field and the interelectronic-interaction effects are accounted for by the perturbation theory. In this way we obtain quantum electrodynamics in the Furry picture. To derive the formal expressions for the perturbation theory terms, we employ the two-time Green-function method [49].

The diagrams, which contribute to the screened self-energy and vacuum-polarization corrections of the first order in α and $1/Z$ in presence of external magnetic field are depicted in Figs. 1 and 2. In order to simplify the derivation we specify the formalism, where the electrons of the closed shell are regarded as belonging to a new redefined vacuum. The redefinition of the vacuum results in replacing $i0$ by $-i0$ in the electron propagator denominators corresponding to the closed shell. In this formalism the one-electron radiative corrections are incorporated together with the interelectronic-interaction contributions. In particular, the one-loop two-electron contributions are merged with the two-loop one-electron contributions. The corresponding diagrams are depicted in Fig. 3. Below we briefly describe the scheme of derivation of the formulas, corresponding to this set of diagrams within the two-time Green-function method. In order to obtain the two-electron corrections one may simply consider the related expressions with the standard definition of the vacuum and then consequently make a replacement

$$\sum_n \frac{|n\rangle\langle n|}{\varepsilon-u\varepsilon_n}\to 2\pi i\delta(\varepsilon-\varepsilon_c)\sum_c|c\rangle\langle c| \tag{2}$$

for each of the electron propagators inside the loops. Here and in the following the notation $u=1-i0$ is used. The summation over c is performed over all electrons of the closed shell.

To zeroth-order approximation the state $|a\rangle$ of the electron is defined by the Dirac equation (1). The energy shift of an isolated level due to the interaction is given by [49]

$$\Delta E_a=\frac{(2\pi i)^{-1}\oint_\Gamma \mathrm{d}E(E-E_a^{(0)})\Delta g_{aa}(E)}{1+(2\pi i)^{-1}\oint_\Gamma \mathrm{d}E\Delta g_{aa}(E)}\,. \tag{3}$$

In our case the unperturbed energy $E_a^{(0)}$ is the Dirac energy ε_a from Eq. (1). The contour Γ surrounds only the pole $E=E_a^{(0)}$, $\Delta g_{aa}(E)=g_{aa}(E)-g_{aa}^{(0)}(E)$, $g_{aa}(E)=\langle\psi_a|g(E)|\psi_a\rangle$, and ψ_a

is the unperturbed wave function. The time-Fourier transform of the Green function is defined as

$$g(E,\mathbf{x}',\mathbf{x})\delta(E-E') = \frac{1}{2\pi i}\int_{-\infty}^{+\infty} \mathrm{d}t\,\mathrm{d}t'\,\exp(iE't'-iEt)\langle 0|T\psi(t',\mathbf{x}')\psi^\dagger(t,\mathbf{x})|0\rangle\,. \tag{4}$$

The Feynman rules for the Green function are given in Ref. [49]. The energy shift ΔE_a and the Green function $g(E)$ are to be expanded as a power series in α,

$$\Delta E_a = \Delta E_a^{(1)} + \Delta E_a^{(2)} + \Delta E_a^{(3)} + \dots\,, \tag{5}$$

$$\Delta g_{aa}(E) = \Delta g_{aa}^{(1)}(E) + \Delta g_{aa}^{(2)}(E) + \Delta g_{aa}^{(3)}(E) + \dots\,. \tag{6}$$

Then from Eq. (3) we find the first-, second- and third-order terms of the energy shift,

$$\Delta E^{(1)} = \frac{1}{2\pi i}\oint_\Gamma \mathrm{d}E(E-E_a^{(0)})\Delta g_{aa}^{(1)}(E)\,, \tag{7}$$

$$\begin{aligned}\Delta E^{(2)} &= \frac{1}{2\pi i}\oint_\Gamma \mathrm{d}E(E-E_a^{(0)})\Delta g_{aa}^{(2)}(E)\\ &- \frac{1}{2\pi i}\oint_\Gamma \mathrm{d}E(E-E_a^{(0)})\Delta g_{aa}^{(1)}(E)\,\frac{1}{2\pi i}\oint_\Gamma \mathrm{d}E'\Delta g_{aa}^{(1)}(E')\,,\end{aligned} \tag{8}$$

$$\begin{aligned}\Delta E^{(3)} &= \frac{1}{2\pi i}\oint_\Gamma \mathrm{d}E(E-E_a^{(0)})\Delta g_{aa}^{(3)}(E)\\ &- \frac{1}{2\pi i}\oint_\Gamma \mathrm{d}E(E-E_a^{(0)})\Delta g_{aa}^{(2)}(E)\,\frac{1}{2\pi i}\oint_\Gamma \mathrm{d}E'\Delta g_{aa}^{(1)}(E')\\ &- \frac{1}{2\pi i}\oint_\Gamma \mathrm{d}E(E-E_a^{(0)})\Delta g_{aa}^{(1)}(E)\\ &\times\left[\frac{1}{2\pi i}\oint_\Gamma \mathrm{d}E'\Delta g_{aa}^{(2)}(E') - \left(\frac{1}{2\pi i}\oint_\Gamma \mathrm{d}E'\Delta g_{aa}^{(1)}(E')\right)^2\right]\,.\end{aligned} \tag{9}$$

Equation (9) and the Feynman rules for $g(E)$ yield the formal expressions for the total contribution of the two-loop diagrams presented in Fig. 3. Consequently replacing each electron propagator according to Eq. (2) we obtain the formal expressions for the two-electron one-loop diagrams displayed in Figs. 1 and 2.

For brevity we introduce the operator

$$I(\omega) = e^2\alpha^\mu\alpha^\nu D_{\mu\nu}(\omega)\,, \tag{10}$$

where $\alpha^\mu = (1,\boldsymbol{\alpha})$ are the Dirac matrices, and $D_{\mu\nu}$ is the photon propagator. It is given by

$$D_{\mu\nu}(\omega,\mathbf{x}_{12}) = g_{\mu\nu}\frac{\exp(i\tilde{\omega}|\mathbf{x}_{12}|)}{4\pi|\mathbf{x}_{12}|}\,, \tag{11}$$

in the Feynman gauge and by

$$\begin{aligned}&D_{00}(\omega,\mathbf{x}_{12}) = \frac{1}{4\pi|\mathbf{x}_{12}|}\,, \qquad D_{i0}(\omega,\mathbf{x}_{12}) = D_{0k}(\omega,\mathbf{x}_{12}) = 0\,,\\ &D_{ik}(\omega,\mathbf{x}_{12}) = \delta_{ik}\frac{\exp(i\tilde{\omega}|\mathbf{x}_{12}|)}{4\pi|\mathbf{x}_{12}|} + \nabla_{1\,i}\nabla_{2\,k}\frac{1-\exp(i\tilde{\omega}|\mathbf{x}_{12}|)}{4\pi\omega^2|\mathbf{x}_{12}|}\,, \qquad (i,k=1,2,3)\,,\end{aligned} \tag{12}$$

in the Coulomb gauge. Here $\mathbf{x}_{12} = \mathbf{x}_1 - \mathbf{x}_2$, $\tilde{\omega} = \sqrt{\omega^2 + i0}$. The branch of the square root is fixed by the condition $\mathrm{Im}\,\tilde{\omega} > 0$. In order to handle the infrared divergencies it is convenient to introduce the photon mass μ. In the Feynman gauge, it results in the replacement $\sqrt{\omega^2 + i0} \to \sqrt{\omega^2 - \mu^2 + i0}$. The limit $\mu \to 0$ should be taken after removing the divergencies. The operator $I(\omega)$ has the following symmetry properties:

$$
\begin{aligned}
&I(\omega) = I(-\omega)\,,\\
&I'(\omega) \equiv \frac{\mathrm{d}}{\mathrm{d}\omega} I(\omega) = -I'(-\omega)\,,\\
&I''(\omega) \equiv \frac{\mathrm{d}^2}{\mathrm{d}^2\omega} I(\omega) = I''(-\omega)\,.
\end{aligned}
\tag{13}
$$

The interaction with the external magnetic field can be represented by an operator T_0. For both cases under consideration (g factor and hyperfine splitting) it is proportional to $[\mathbf{r} \times \boldsymbol{\alpha}]_z$, what defines the angular momentum structure. Explicit formulas for T_0 will be given in Sec. V.

III. SCREENED SELF-ENERGY

The diagrams of the screened self-energy correction, corresponding to the first term in Eq. (9), are shown in Fig. 1. We divide the total contribution of these diagrams into the reducible and irreducible parts. The irreducible part is the sum of the terms where the energies of the intermediate states are different from the energy of the initial state. The reducible part is the remainder. We denote the irreducible parts of each diagram A – F by the same letter: $\Delta E^{\mathrm{SE}(A-F)}_{\mathrm{SQED}}$. It is convenient to divide them into three groups, according to the number of the ω-dependent denominators (ω is the virtual photon energy, over which the integration is performed). The terms with only one denominator (A, B and E) are referred to as a "modified self-energy" terms, since all of them have the form of a matrix element of the self-energy operator, $\langle X|\Sigma(\varepsilon)|Y\rangle$. The terms with two denominators (C and F) are denoted as a "modified vertex", and the diagram D with three denominators is denoted as a "double-vertex". The reducible parts are considered together with the related contributions that arise from the second and the third terms in Eq. (9). Their sum is divided into three parts: G, H, and I, according to the number of the ω-dependent denominators. These three parts are considered together with the "modified self-energy", "modified vertex", and "double-vertex" terms, respectively. Finally, the total contribution of the two-electron self-energy

diagrams is given by

$$\Delta E^{\rm SE}_{\rm SQED} = \sum_b \sum_{PQ} (-1)^{P+Q} \Big(\Delta E^{{\rm SE}(A)}_{\rm SQED} + \Delta E^{{\rm SE}(B)}_{\rm SQED} + \Delta E^{{\rm SE}(C)}_{\rm SQED} + \Delta E^{{\rm SE}(D)}_{\rm SQED} + \Delta E^{{\rm SE}(E)}_{\rm SQED} + \Delta E^{{\rm SE}(F)}_{\rm SQED} + \Delta E^{{\rm SE}(G)}_{\rm SQED} + \Delta E^{{\rm SE}(H)}_{\rm SQED} + \Delta E^{{\rm SE}(I)}_{\rm SQED} \Big) \,. \tag{14}$$

Here P and Q are the permutation operators, interchanging the valence (a) and the core (b) electron states, $(-1)^P$ is the sign of the permutation P. The summation over b runs over two core electron states with different projections of the total angular momentum. In what follows, we will also use the notation $\Delta \equiv \varepsilon_{Qb} - \varepsilon_{Pb}$.

One has to pay special attention to the ultraviolet (UV) divergencies, that arise in the formal expressions under consideration. First, we introduce the unrenormalized self-energy operator,

$$\langle p|\Sigma(\varepsilon)|q\rangle = \frac{i}{2\pi} \int {\rm d}\omega \sum_n \frac{\langle pn|I(\omega)|nq\rangle}{\varepsilon - \omega - u\varepsilon_n} \,. \tag{15}$$

Here and below the integration over ω is carried out from $-\infty$ to $+\infty$. Every diagram involving the self-energy loop has to be considered together with the corresponding diagram with the mass counterterm, what results in the replacement $\Sigma(\varepsilon) \to \Sigma_{\rm R}(\varepsilon) = \Sigma(\varepsilon) - \gamma^0 \delta m$. The matrix elements of $\Sigma_{\rm R}(\varepsilon)$ still have the divergent part:

$$\langle p|\Sigma_{\rm R}(\varepsilon)|q\rangle = B^{(1)} \langle p| \left[\varepsilon - \boldsymbol{\alpha}\cdot\mathbf{p} - \beta m - V(\mathbf{x})\right] |q\rangle + \text{finite part} \,, \tag{16}$$

where $B^{(1)}$ is the UV-divergent constant. Assuming that $|p\rangle$ and $|q\rangle$ obey the Dirac equation (1) we have,

$$\langle p|\Sigma_{\rm R}(\varepsilon)|q\rangle = B^{(1)}(\varepsilon - \varepsilon_p)\delta_{pq} + \text{finite part} \,. \tag{17}$$

In order to isolate the divergent part we follow the potential-expansion approach [50]. The finite part of the self-energy matrix element is then divided into the zero- and one-potential terms evaluated in momentum space, and the many-potential term evaluated in coordinate space. The diagrams with one vertex inside the self-energy loop also suffer from UV-divergencies. It can be shown that for an arbitrary operator U,

$$\frac{i}{2\pi} \int {\rm d}\omega \sum_{n_{1,2}} \frac{\langle pn_2|I(\omega)|n_1 q\rangle \langle n_1|U|n_2\rangle}{(\varepsilon - \omega - u\varepsilon_{n_1})(\varepsilon - \omega - u\varepsilon_{n_2})} = L^{(1)} \langle p|U|q\rangle + \text{finite part} \,. \tag{18}$$

In our case U is either T_0 or $I(\Delta)$ (in the latter case $\langle p|U|q\rangle \equiv \langle pr|I(\Delta)|qs\rangle$). Due to the Ward identity we have $L^{(1)} = -B^{(1)}$. The finite part of the vertex contributions is divided into the zero-potential term evaluated in momentum space and the many-potential term evaluated in coordinate space.

From Eq. (17) one can see that for the first-order self-energy correction the divergent part is zero. However, in case of the higher-order diagrams under consideration the contributions of particular diagrams are divergent. Nevertheless, as it is shown below, the sum of all the contributions to the screened self-energy correction is finite.

A. "Modified self-energy" diagrams

The irreducible parts of the diagrams A, B and E can be presented as the matrix elements of the self-energy operator $\langle X|\Sigma(\varepsilon)|Y\rangle$ with various wave functions $\langle X|$ and $|Y\rangle$. The formulas for these contributions are as follows,

$$\Delta E^{\mathrm{SE}(A)}_{\mathrm{SQED}} = \Delta E^{\mathrm{SE}(A1)}_{\mathrm{SQED}} + \Delta E^{\mathrm{SE}(A2)}_{\mathrm{SQED}}\,, \tag{19}$$

$$\Delta E^{\mathrm{SE}(A1)}_{\mathrm{SQED}} = 2\sum_{n_{1,2}}{}' \langle Pa|\Sigma(\varepsilon_{Pa})|n_1\rangle \frac{\langle n_1|T_0|n_2\rangle\langle n_2 Pb|I(\Delta)|QaQb\rangle}{(\varepsilon_{Pa}-\varepsilon_{n_1})(\varepsilon_{Pa}-\varepsilon_{n_2})}\,, \tag{20}$$

$$\Delta E^{\mathrm{SE}(A2)}_{\mathrm{SQED}} = 2\sum_{n_{1,2}}{}' \langle Pa|\Sigma(\varepsilon_{Pa})|n_1\rangle \frac{\langle n_1 Pb|I(\Delta)|n_2Qb\rangle\langle n_2|T_0|Qa\rangle}{(\varepsilon_{Pa}-\varepsilon_{n_1})(\varepsilon_{Qa}-\varepsilon_{n_2})}\,, \tag{21}$$

$$\Delta E^{\mathrm{SE}(B)}_{\mathrm{SQED}} = 2\sum_{n_{1,2}}{}' \frac{\langle Pa|T_0|n_1\rangle}{\varepsilon_{Pa}-\varepsilon_{n_1}} \langle n_1|\Sigma(\varepsilon_{Pa})|n_2\rangle \frac{\langle n_2 Pb|I(\Delta)|QaQb\rangle}{\varepsilon_{Pa}-\varepsilon_{n_2}}\,, \tag{22}$$

$$\Delta E^{\mathrm{SE}(E)}_{\mathrm{SQED}} = \Delta E^{\mathrm{SE}(E1)}_{\mathrm{SQED}} + \Delta E^{\mathrm{SE}(E2)}_{\mathrm{SQED}}\,, \tag{23}$$

$$\Delta E^{\mathrm{SE}(E1)}_{\mathrm{SQED}} = 2\sum_{n_{1,2}}{}' \langle Pa|\Sigma(\varepsilon_{Pa})|n_1\rangle \frac{\langle Pb|T_0|n_2\rangle\langle n_1 n_2|I(\Delta)|QaQb\rangle}{(\varepsilon_{Pa}-\varepsilon_{n_1})(\varepsilon_{Pb}-\varepsilon_{n_2})}\,, \tag{24}$$

$$\Delta E^{\mathrm{SE}(E2)}_{\mathrm{SQED}} = 2\sum_{n_{1,2}}{}' \langle Pa|\Sigma(\varepsilon_{Pa})|n_1\rangle \frac{\langle n_1 Pb|I(\Delta)|Qan_2\rangle\langle n_2|T_0|Qb\rangle}{(\varepsilon_{Pa}-\varepsilon_{n_1})(\varepsilon_{Qb}-\varepsilon_{n_2})}\,. \tag{25}$$

All the reducible terms of the similar structure are denoted as $\Delta E^{\mathrm{SE}(G)}_{\mathrm{SQED}}$,

$$\Delta E^{\mathrm{SE}(G)}_{\mathrm{SQED}} = \Delta E^{\mathrm{SE}(G1)}_{\mathrm{SQED}} + \Delta E^{\mathrm{SE}(G2)}_{\mathrm{SQED}} + \Delta E^{\mathrm{SE}(G3)}_{\mathrm{SQED}}\,, \tag{26}$$

$$\begin{aligned}\Delta E^{\mathrm{SE}(G1)}_{\mathrm{SQED}} = -2\sum_{n_1}{}' \frac{1}{(\varepsilon_{Pa}-\varepsilon_{n_1})^2}\Big[&\langle Pa|\Sigma(\varepsilon_{Pa})|n_1\rangle\langle n_1|T_0|Pa\rangle\langle PaPb|I(\Delta)|QaQb\rangle \\ &+\langle Pa|\Sigma(\varepsilon_{Pa})|n_1\rangle\langle n_1 Pb|I(\Delta)|QaQb\rangle\langle Pa|T_0|Pa\rangle \\ &+\langle Pa|\Sigma(\varepsilon_{Pa})|Pa\rangle\langle Pa|T_0|n_1\rangle\langle n_1 Pb|I(\Delta)|QaQb\rangle\Big]\,,\end{aligned} \tag{27}$$

$$\Delta E^{\mathrm{SE}(G2)}_{\mathrm{SQED}} = 2\sum_{n_1}{}' \frac{1}{\varepsilon_{Pa}-\varepsilon_{n_1}}\Big[\langle Pa|\Sigma(\varepsilon_{Pa})|n_1\rangle\langle n_1|T_0|Pa\rangle\langle PaPb|I'(\Delta)|QaQb\rangle$$
$$+\langle Pa|\Sigma(\varepsilon_{Pa})|n_1\rangle\langle n_1Pb|I'(\Delta)|QaQb\rangle\Big(\langle Qb|T_0|Qb\rangle - \langle Pb|T_0|Pb\rangle\Big)\Big]$$
$$+2\,\langle Pa|\Sigma(\varepsilon_{Pa})|Pa\rangle\sum_{n_1}{}'\left[\frac{\langle PaPb|I'(\Delta)|n_1Qb\rangle\langle n_1|T_0|Qa\rangle}{\varepsilon_{Qa}-\varepsilon_{n_1}}\right.$$
$$\left.+\frac{\langle PaPb|I'(\Delta)|Qan_1\rangle\langle n_1|T_0|Qb\rangle}{\varepsilon_{Qb}-\varepsilon_{n_1}}\right], \qquad (28)$$

$$\Delta E^{\mathrm{SE}(G3)}_{\mathrm{SQED}} = \langle Pa|\Sigma(\varepsilon_{Pa})|Pa\rangle\langle PaPb|I''(\Delta)|QaQb\rangle\Big(\langle Qb|T_0|Qb\rangle - \langle Pb|T_0|Pb\rangle\Big). \qquad (29)$$

Equations (19)–(29) possess ultraviolet (UV) divergences. Taking into account the mass counterterm and employing Eq. (17) we find that $\Delta E^{\mathrm{SE}(B)}_{\mathrm{SQED}}$ has a non-zero UV-divergent part,

$$\Delta E^{\mathrm{SE}(B)}_{\mathrm{SQED}}(\mathrm{UV}) = 2\,B^{(1)}\sum_{n_1}{}'\frac{\langle Pa|T_0|n_1\rangle\langle n_1Pb|I(\Delta)|QaQb\rangle}{\varepsilon_{Pa}-\varepsilon_{n_1}}. \qquad (30)$$

By the end of the next subsection we will show that the sum of all the UV-divergent terms is zero.

B. "Modified vertex" diagrams

For the irreducible parts of the diagrams C and F we have,

$$\Delta E^{\mathrm{SE}(C)}_{\mathrm{SQED}} = \Delta E^{\mathrm{SE}(C1)}_{\mathrm{SQED}} + \Delta E^{\mathrm{SE}(C2)}_{\mathrm{SQED}}, \qquad (31)$$

$$\Delta E^{\mathrm{SE}(C1)}_{\mathrm{SQED}} = 2\,\frac{i}{2\pi}\int \mathrm{d}\omega \sum_{n_{1,2,3}}^{\varepsilon_{n_3}\neq\varepsilon_{Pa}} \frac{\langle Pan_2|I(\omega)|n_1n_3\rangle\langle n_1|T_0|n_2\rangle}{(\varepsilon_{Pa}-\omega-u\varepsilon_{n_1})(\varepsilon_{Pa}-\omega-u\varepsilon_{n_2})}\frac{\langle n_3Pb|I(\Delta)|QaQb\rangle}{(\varepsilon_{Pa}-\varepsilon_{n_3})}, \qquad (32)$$

$$\Delta E^{\mathrm{SE}(C2)}_{\mathrm{SQED}} = 2\,\frac{i}{2\pi}\int \mathrm{d}\omega \sum_{n_{1,2,3}}^{\varepsilon_{n_3}\neq\varepsilon_{Qa}} \frac{\langle Pan_2|I(\omega)|n_1n_3\rangle\langle n_1Pb|I(\Delta)|n_2Qb\rangle}{(\varepsilon_{Pa}-\omega-u\varepsilon_{n_1})(\varepsilon_{Qa}-\omega-u\varepsilon_{n_2})}\frac{\langle n_3|T_0|Qa\rangle}{(\varepsilon_{Qa}-\varepsilon_{n_3})}, \qquad (33)$$

$$\Delta E^{\mathrm{SE}(F)}_{\mathrm{SQED}} = 2\,\frac{i}{2\pi}\int \mathrm{d}\omega \sum_{n_{1,2,3}}^{\varepsilon_{n_3}\neq\varepsilon_{Qb}} \frac{\langle Pan_2|I(\omega)|n_1Qa\rangle\langle n_1Pb|I(\Delta)|n_2n_3\rangle}{(\varepsilon_{Pa}-\omega-u\varepsilon_{n_1})(\varepsilon_{Qa}-\omega-u\varepsilon_{n_2})}\frac{\langle n_3|T_0|Qb\rangle}{(\varepsilon_{Qb}-\varepsilon_{n_3})}. \qquad (34)$$

Since these diagrams have one vertex inside the self-energy loop, the corresponding expressions have the following structure of the ω-dependent denominators: $(\Delta_1-\omega)^{-1}(\Delta_2-\omega)^{-1}$. All the reducible terms that have similar structure are denoted as $\Delta E^{\mathrm{SE}(H)}_{\mathrm{SQED}}$,

$$\Delta E^{\mathrm{SE}(H)}_{\mathrm{SQED}} = \Delta E^{\mathrm{SE}(H1)}_{\mathrm{SQED}} + \Delta E^{\mathrm{SE}(H2)}_{\mathrm{SQED}} + \Delta E^{\mathrm{SE}(H3)}_{\mathrm{SQED}}, \qquad (35)$$

$$\Delta E^{\mathrm{SE}(H1)}_{\mathrm{SQED}} = \frac{i}{2\pi}\int \mathrm{d}\omega \sum_{n_{1,2}} \frac{\langle Pan_2|I(\omega)|n_1Pa\rangle\langle n_1|T_0|n_2\rangle}{(\varepsilon_{Pa}-\omega-u\varepsilon_{n_1})(\varepsilon_{Pa}-\omega-u\varepsilon_{n_2})}\langle PaPb|I'(\Delta)|QaQb\rangle\,, \quad (36)$$

$$\Delta E^{\mathrm{SE}(H2)}_{\mathrm{SQED}} = \frac{i}{2\pi}\int \mathrm{d}\omega \sum_{n_{1,2}} \frac{\langle Pan_2|I(\omega)|n_1Qa\rangle\langle n_1Pb|I'(\Delta)|n_2Qb\rangle}{(\varepsilon_{Pa}-\omega-u\varepsilon_{n_1})(\varepsilon_{Qa}-\omega-u\varepsilon_{n_2})} \times\Big(\langle Qb|T_0|Qb\rangle - \langle Pb|T_0|Pb\rangle\Big)\,, \quad (37)$$

$$\begin{aligned}\Delta E^{\mathrm{SE}(H3)}_{\mathrm{SQED}} = 2\sum_{n_1}{}' \frac{1}{\varepsilon_{Pa}-\varepsilon_{n_1}}\Big[&\langle Pa|\Sigma'(\varepsilon_{Pa})|n_1\rangle\langle n_1|T_0|Pa\rangle\langle PaPb|I(\Delta)|QaQb\rangle \\ &+\langle Pa|\Sigma'(\varepsilon_{Pa})|n_1\rangle\langle n_1Pb|I(\Delta)|QaQb\rangle\langle Pa|T_0|Pa\rangle\Big] \\ &+\langle Pa|\Sigma'(\varepsilon_{Pa})|Pa\rangle\left\{2\sum_{n_1}{}'\left[\frac{\langle Pa|T_0|n_1\rangle\langle n_1Pb|I(\Delta)|QaQb\rangle}{\varepsilon_{Pa}-\varepsilon_{n_1}}\right.\right. \\ &\left.+\frac{\langle Pb|T_0|n_1\rangle\langle Pan_1|I(\Delta)|QaQb\rangle}{\varepsilon_{Pb}-\varepsilon_{n_1}}\right] \\ &\left.+\langle PaPb|I'(\Delta)|QaQb\rangle\Big(\langle Pa|T_0|Pa\rangle+\langle Qb|T_0|Qb\rangle-\langle Pb|T_0|Pb\rangle\Big)\right\}\,. \end{aligned} \quad (38)$$

Equations (31)–(38) diverge both in ultraviolet and infrared regions. The UV-divergent terms are:

$$\Delta E^{\mathrm{SE}(C1)}_{\mathrm{SQED}}(\mathrm{UV}) = 2\,L^{(1)}\sum_{n_1}{}'\frac{\langle Pa|T_0|n_1\rangle\langle n_1Pb|I(\Delta)|QaQb\rangle}{\varepsilon_{Pa}-\varepsilon_{n_1}}\,, \quad (39)$$

$$\Delta E^{\mathrm{SE}(C2)}_{\mathrm{SQED}}(\mathrm{UV}) = 2\,L^{(1)}\sum_{n_1}{}'\frac{\langle PaPb|I(\Delta)|n_1Qb\rangle\langle n_1|T_0|Qa\rangle}{\varepsilon_{Qa}-\varepsilon_{n_1}}\,, \quad (40)$$

$$\Delta E^{\mathrm{SE}(F)}_{\mathrm{SQED}}(\mathrm{UV}) = 2\,L^{(1)}\sum_{n_1}{}'\frac{\langle PaPb|I(\Delta)|Qan_1\rangle\langle n_1|T_0|Qb\rangle}{\varepsilon_{Qb}-\varepsilon_{n_1}}\,, \quad (41)$$

$$\Delta E^{\mathrm{SE}(H1)}_{\mathrm{SQED}}(\mathrm{UV}) = L^{(1)}\,\langle Pa|T_0|Pa\rangle\langle PaPb|I'(\Delta)|QaQb\rangle\,, \quad (42)$$

$$\Delta E^{\mathrm{SE}(H2)}_{\mathrm{SQED}}(\mathrm{UV}) = L^{(1)}\,\langle PaPb|I'(\Delta)|QaQb\rangle\Big(\langle Qb|T_0|Qb\rangle-\langle Pb|T_0|Pb\rangle\Big)\,, \quad (43)$$

$$\begin{aligned}\Delta E^{\mathrm{SE}(H3)}_{\mathrm{SQED}}(\mathrm{UV}) = 2\,B^{(1)}\sum_{n_1}{}'\Bigg(&\frac{\langle Pa|T_0|n_1\rangle\langle n_1Pb|I(\Delta)|QaQb\rangle}{\varepsilon_{Pa}-\varepsilon_{n_1}} \\ &+\frac{\langle Pb|T_0|n_1\rangle\langle Pan_1|I(\Delta)|QaQb\rangle}{\varepsilon_{Pb}-\varepsilon_{n_1}}\Bigg) \\ +B^{(1)}\,\langle PaPb|I'(\Delta)|QaQb\rangle&\Big(\langle Pa|T_0|Pa\rangle+\langle Qb|T_0|Qb\rangle-\langle Pb|T_0|Pb\rangle\Big)\,. \end{aligned} \quad (44)$$

One can see that the sum of the UV-divergent terms (30), (39)–(44) is zero.

There are also infrared (IR) divergencies in Eqs. (31)–(38). They arise when the energies of the intermediate states n are equal to the energies of the reference states a or b, what leads to the factor $1/(\omega - i0)^2$. In order to handle these divergencies we introduce a non-zero photon mass μ and isolate analytically the terms proportional to $\ln \mu$. Similar terms arise in Eqs. (45)–(46) and should be considered together to yield a finite result.

C. "Double-vertex" diagrams

Finally, we consider the diagram D with two vertices inside the self-energy loop,

$$\Delta E^{\mathrm{SE}(D)}_{\mathrm{SQED}} = 2\frac{i}{2\pi}\int \mathrm{d}\omega \sum_{n_{1,2,3}} \frac{\langle Pan_3|I(\omega)|n_1Qa\rangle\langle n_1Pb|I(\Delta)|n_2Qb\rangle\langle n_2|T_0|n_3\rangle}{(\varepsilon_{Pa}-\omega-u\varepsilon_{n_1})(\varepsilon_{Qa}-\omega-u\varepsilon_{n_2})(\varepsilon_{Qa}-\omega-u\varepsilon_{n_3})}\,. \tag{45}$$

The reducible contributions with the third power of ω in the denominators are denoted as $\Delta E^{\mathrm{SE}(I)}_{\mathrm{SQED}}$,

$$\Delta E^{\mathrm{SE}(I)}_{\mathrm{SQED}} = \Delta E^{\mathrm{SE}(I1)}_{\mathrm{SQED}} + \Delta E^{\mathrm{SE}(I2)}_{\mathrm{SQED}} + \Delta E^{\mathrm{SE}(I3)}_{\mathrm{SQED}}\,, \tag{46}$$

$$\begin{aligned}\Delta E^{\mathrm{SE}(I1)}_{\mathrm{SQED}} = &-\frac{i}{2\pi}\int \mathrm{d}\omega \sum_{n_{1,2}} \frac{\langle Pan_2|I(\omega)|n_1Pa\rangle\langle n_1|T_0|n_2\rangle}{(\varepsilon_{Pa}-\omega-u\varepsilon_{n_1})(\varepsilon_{Pa}-\omega-u\varepsilon_{n_2})}\\ &\times\left(\frac{1}{\varepsilon_{Pa}-\omega-u\varepsilon_{n_1}}+\frac{1}{\varepsilon_{Pa}-\omega-u\varepsilon_{n_2}}\right)\langle PaPb|I(\Delta)|QaQb\rangle\,,\end{aligned} \tag{47}$$

$$\begin{aligned}\Delta E^{\mathrm{SE}(I2)}_{\mathrm{SQED}} = &-\frac{i}{2\pi}\int \mathrm{d}\omega \sum_{n_{1,2}} \frac{\langle Pan_2|I(\omega)|n_1Qa\rangle\langle n_1Pb|I(\Delta)|n_2Qb\rangle}{(\varepsilon_{Pa}-\omega-u\varepsilon_{n_1})(\varepsilon_{Qa}-\omega-u\varepsilon_{n_2})}\\ &\times\left(\frac{\langle Pa|T_0|Pa\rangle}{\varepsilon_{Pa}-\omega-u\varepsilon_{n_1}}+\frac{\langle Qa|T_0|Qa\rangle}{\varepsilon_{Qa}-\omega-u\varepsilon_{n_2}}\right)\,,\end{aligned} \tag{48}$$

$$\Delta E^{\mathrm{SE}(I3)}_{\mathrm{SQED}} = \langle Pa|\Sigma''(\varepsilon_{Pa})|Pa\rangle\langle Pa|T_0|Pa\rangle\langle PaPb|I(\Delta)|QaQb\rangle\,. \tag{49}$$

These contributions are UV-finite. However, they contain IR-divergent terms that should be considered together with similar terms from Eqs. (32)–(35). Introducing a non-zero photon mass μ and isolating the terms, proportional to $\ln \mu$ we find that the sum of all the IR-divergent terms from the terms C, F, H, D and I is finite.

D. Numerical evaluation

Evaluation of the two-electron self-energy correction requires momentum-space calculation of the zero- and one-potential terms of the "modified self-energy" contributions ($\Delta E^{\mathrm{SE}(A)}_{\mathrm{SQED}}$, $\Delta E^{\mathrm{SE}(B)}_{\mathrm{SQED}}$, $\Delta E^{\mathrm{SE}(E)}_{\mathrm{SQED}}$, and $\Delta E^{\mathrm{SE}(G)}_{\mathrm{SQED}}$) and zero-potential terms of the "modified vertex" contributions ($\Delta E^{\mathrm{SE}(C)}_{\mathrm{SQED}}$, $\Delta E^{\mathrm{SE}(F)}_{\mathrm{SQED}}$, and $\Delta E^{\mathrm{SE}(H)}_{\mathrm{SQED}}$). For the zero- and one-potential terms of the "modified self-energy" contributions we employ the numerical procedure, developed for the self-energy diagram [51, 52].

The "magnetic-vertex" part (with the operator T_0 in the vertex) of the "modified vertex" contributions is somewhat similar to the vertex part of the one-electron self-energy correction to the g factor or the hyperfine splitting. Hence, our treatment of its zero-potential term is based on the corresponding calculational procedures developed in Ref. [14] for the g factor and in Refs. [9, 36] for the hyperfine splitting. The angular integration, however, required significant generalization, in both cases, due to the interelectronic-interaction matrix elements. The "interaction-vertex" part (with the interelectronic-interaction operator $I(\Delta)$ in the vertex) resembles the vertex part of the two-electron self-energy correction to the energy levels. Therefore, we have developed the numerical algorithm for the corresponding zero-potential term on the basis of the one presented in Ref. [53]. The main difference is the structure of the angular integrals which is substantially more complicated, due to the interaction with the external magnetic field.

The many-potential terms of the "modified self-energy" and "modified vertex" parts, as well as the complete contribution of the "double vertex" part are calculated in the coordinate space. Angular integration and summation over intermediate angular momentum projections is carried out in the standard way. The summation over the complete spectrum of the Dirac equation at fixed angular quantum numbers $\kappa_{1,2,3}$ is performed using the dual-kinetic-balance (DKB) approach [54] with the basis functions constructed from B-splines [55]. The infinite summation over $\kappa_{1,2,3}$ is terminated at $|\kappa| = 10$–15 and the rest of the sum is evaluated by the least-square inverse-polynomial fitting. In order to perform the integration over ω we employ two different contours, thus performing an additional cross-check. Both of them involve the Wick rotation. The first contour is the same as in Ref. [51]. The integration is performed along the imaginary axis. Besides, the contributions from the poles arising from the terms with $\varepsilon_n \leq \varepsilon_{a,b}$ must be calculated. The advantage of this contour is that the calculation is less time-consuming, in particular, due to the fact that $\mathrm{Im}[I(\omega)] = 0$ when $\mathrm{Re}[\omega] = 0$. The second contour was proposed in Ref. [52]. The

integration is performed along the line $C_{\rm H}$ $[\omega_0 - i\infty, \omega_0 + i\infty]$ and along the half-ellipse $C_{\rm L}$, going between 0 and ω_0 in the lower half-plane. The advantage of this contour is that one does not need to investigate the pole-structure of the integrand, which is especially complicated for the diagram D.

In order to check the numerical procedure we have performed the calculation in both Feynman and Coulomb gauges for the photon propagator corresponding to the interelectronic interaction. The individual terms A–I are presented in both gauges for the g factor of $^{208}\mathrm{Pb}^{79+}$ in Table I and for the hyperfine splitting of $^{209}\mathrm{Bi}^{83+}$ in Table II. The data for the g factor demonstrate large cancellation of the individual terms, leading to the loss of 2 digits in the total value. Due to this fact the uncertainty of our results for the g factor is significantly larger than the one for the hyperfine splitting. Moreover, for lower values of Z the convergence of the partial-wave expansion worsen, and the resulting accuracy becomes unacceptable. This means that for the g factor in the middle-Z region a special treatment of the many potential term is required.

IV. TWO-ELECTRON VACUUM POLARIZATION

The diagrams, corresponding to the screened vacuum-polarization correction, are shown in Fig. 2. Similar to the case of the screened self-energy we divide the total contribution of these diagrams into the irreducible and reducible parts. The reducible part should be considered together with the related contributions from the second and the third terms in Eq. (9). The irreducible parts of each diagram A – F are denoted by the same letter, $\Delta E^{{\rm VP}(A-F)}_{\rm SQED}$, while the reducible terms are collected into three groups, $\Delta E^{{\rm VP}(G,H,I)}_{\rm SQED}$. The total correction due to the screened vacuum-polarization is given by

$$\Delta E^{\rm VP}_{\rm SQED} = \sum_b \sum_{PQ} (-1)^{P+Q} \Big(\Delta E^{{\rm VP}(A)}_{\rm SQED} + \Delta E^{{\rm VP}(B)}_{\rm SQED} + \Delta E^{{\rm VP}(C)}_{\rm SQED} + \Delta E^{{\rm VP}(D)}_{\rm SQED} + \Delta E^{{\rm VP}(E)}_{\rm SQED} + \Delta E^{{\rm VP}(F)}_{\rm SQED} + \Delta E^{{\rm VP}(G)}_{\rm SQED} + \Delta E^{{\rm VP}(H)}_{\rm SQED} + \Delta E^{{\rm VP}(I)}_{\rm SQED} \Big) \,. \tag{50}$$

Here again P and Q are the permutation operators, interchanging a and b, and the summation over b runs over all core electron states. The notation $\Delta \equiv \varepsilon_{Qb} - \varepsilon_{Pb}$ will be used below.

The diagrams A, B and E (so-called 'electric-loop' diagrams) involve the matrix elements of the standard Coulomb-field-induced vacuum-polarization potential $U^{\rm el}_{\rm VP}$. The charge renormalization makes this potential finite, and the expressions for the resulting contributions, Uehling and

Wichmann-Kroll potentials, can be found, e.g., in Ref. [56]. The contributions of these diagrams are given by

$$\Delta E^{\mathrm{VP}(A)}_{\mathrm{SQED}} = \Delta E^{\mathrm{VP}(A1)}_{\mathrm{SQED}} + \Delta E^{\mathrm{VP}(A2)}_{\mathrm{SQED}}\,, \tag{51}$$

$$\Delta E^{\mathrm{VP}(A1)}_{\mathrm{SQED}} = 2\sum_{n_{1,2}}{}' \langle Pa|U^{\mathrm{el}}_{\mathrm{VP}}|n_1\rangle \frac{\langle n_1|T_0|n_2\rangle\langle n_2 Pb|I(\Delta)|QaQb\rangle}{(\varepsilon_{Pa}-\varepsilon_{n_1})(\varepsilon_{Pa}-\varepsilon_{n_2})}\,, \tag{52}$$

$$\Delta E^{\mathrm{VP}(A2)}_{\mathrm{SQED}} = 2\sum_{n_{1,2}}{}' \langle Pa|U^{\mathrm{el}}_{\mathrm{VP}}|n_1\rangle \frac{\langle n_1 Pb|I(\Delta)|n_2Qb\rangle\langle n_2|T_0|Qa\rangle}{(\varepsilon_{Pa}-\varepsilon_{n_1})(\varepsilon_{Qa}-\varepsilon_{n_2})}\,, \tag{53}$$

$$\Delta E^{\mathrm{VP}(B)}_{\mathrm{SQED}} = 2\sum_{n_{1,2}}{}' \frac{\langle Pa|T_0|n_1\rangle}{\varepsilon_{Pa}-\varepsilon_{n_1}} \langle n_2|U^{\mathrm{el}}_{\mathrm{VP}}|n_1\rangle \frac{\langle n_2 Pb|I(\Delta)|QaQb\rangle}{\varepsilon_{Pa}-\varepsilon_{n_2}}\,, \tag{54}$$

$$\Delta E^{\mathrm{VP}(E)}_{\mathrm{SQED}} = \Delta E^{\mathrm{VP}(E1)}_{\mathrm{SQED}} + \Delta E^{\mathrm{VP}(E2)}_{\mathrm{SQED}}\,, \tag{55}$$

$$\Delta E^{\mathrm{VP}(E1)}_{\mathrm{SQED}} = 2\sum_{n_{1,2}}{}' \langle Pa|U^{\mathrm{el}}_{\mathrm{VP}}|n_1\rangle \frac{\langle Pb|T_0|n_2\rangle\langle n_1 n_2|I(\Delta)|QaQb\rangle}{(\varepsilon_{Pa}-\varepsilon_{n_1})(\varepsilon_{Pb}-\varepsilon_{n_2})}\,, \tag{56}$$

$$\Delta E^{\mathrm{VP}(E2)}_{\mathrm{SQED}} = 2\sum_{n_{1,2}}{}' \langle Pa|U^{\mathrm{el}}_{\mathrm{VP}}|n_1\rangle \frac{\langle n_1 Pb|I(\Delta)|Qan_2\rangle\langle n_2|T_0|Qb\rangle}{(\varepsilon_{Pa}-\varepsilon_{n_1})(\varepsilon_{Qb}-\varepsilon_{n_2})}\,. \tag{57}$$

The diagrams of type C (so-called 'magnetic-loop' diagrams) involve the matrix elements of the magnetic-field-induced vacuum-polarization potential $U^{\mathrm{ml}}_{\mathrm{VP}}$. It also requires the charge renormalization to make it finite. Our present treatment of this potential is restricted to the Uehling (free-electron-loop) approximation. The expression for this potential in the Uehling approximation in case of the hyperfine interaction can be found in Ref. [57] for the point-dipole nuclear model, and in Ref. [47] for the sphere model of the nuclear magnetization distribution. In case of the g factor this potential in the Uehling approximation is equal to zero. The contribution of the diagrams of type C is given by

$$\Delta E^{\mathrm{VP}(C)}_{\mathrm{SQED}} = 2\sum_{n_1}{}' \langle Pa|U^{\mathrm{ml}}_{\mathrm{VP}}|n_1\rangle \frac{\langle n_1 Pb|I(\Delta)|QaQb\rangle}{\varepsilon_{Pa}-\varepsilon_{n_1}}\,. \tag{58}$$

The diagram of type F contains the interelectronic-interaction operator modified by the vacuum polarization $I_{\mathrm{VP}}(\omega)$. Our present treatment of this term is restricted to the Uehling approximation.

The corresponding expression for $I_{\rm VP}(\omega)$ in the Feynman gauge can be found, e.g., in Ref. [58]. The contribution of this diagram reads

$$\Delta E^{{\rm VP}(F)}_{\rm SQED} = 2\sum_{n_1}{}' \frac{\langle Pa|T_0|n_1\rangle}{\varepsilon_{Pa}-\varepsilon_{n_1}}\langle n_1 Pb|I_{\rm VP}(\Delta)|QaQb\rangle\,. \tag{59}$$

The contribution of the diagram D is given by the expression

$$\Delta E^{{\rm VP}(D)}_{\rm SQED} = \langle PaPb|I^{\rm ml}_{\rm VP}(\Delta)|QaQb\rangle\,, \tag{60}$$

where the operator $I^{\rm ml}_{\rm VP}$ can be derived within the two-time Green function method. In the present work we omit this term, assuming its value is relatively small.

The reducible contributions G, H and I are given by

$$\Delta E^{{\rm VP}(G)}_{\rm SQED} = \Delta E^{{\rm VP}(G1)}_{\rm SQED} + \Delta E^{{\rm VP}(G2)}_{\rm SQED} + \Delta E^{{\rm VP}(G3)}_{\rm SQED}\,, \tag{61}$$

$$\begin{aligned}\Delta E^{{\rm VP}(G1)}_{\rm SQED} = -2\sum_{n_1}{}' \frac{1}{(\varepsilon_{Pa}-\varepsilon_{n_1})^2}\Big\{&\langle Pa|U^{\rm el}_{\rm VP}|n_1\rangle\langle n_1|T_0|Pa\rangle\langle PaPb|I(\Delta)|QaQb\rangle\\ &+\langle Pa|U^{\rm el}_{\rm VP}|Pa\rangle\langle Pa|T_0|n_1\rangle\langle n_1Pb|I(\Delta)|QaQb\rangle\\ &+\langle Pa|T_0|Pa\rangle\langle Pa|U^{\rm el}_{\rm VP}|n_1\rangle\langle n_1Pb|I(\Delta)|QaQb\rangle\Big\}\,,\end{aligned} \tag{62}$$

$$\begin{aligned}\Delta E^{{\rm VP}(G2)}_{\rm SQED} = 2\Bigg\{\sum_{n_1}{}' \frac{1}{\varepsilon_{Pa}-\varepsilon_{n_1}}\Big[&\langle Pa|U^{\rm el}_{\rm VP}|n_1\rangle\langle n_1|T_0|Pa\rangle\langle PaPb|I'(\Delta)|QaQb\rangle\\ &+\langle Pa|U^{\rm el}_{\rm VP}|n_1\rangle\langle n_1Pb|I'(\Delta)|QaQb\rangle\Big(\langle Qb|T_0|Qb\rangle-\langle Pb|T_0|Pb\rangle\Big)\Big]\\ &+\langle Pa|U^{\rm el}_{\rm VP}|Pa\rangle\Bigg[\sum_{n_1}{}'\frac{\langle PaPb|I'(\Delta)|n_1Qb\rangle\langle n_1|T_0|Qa\rangle}{\varepsilon_{Qa}-\varepsilon_{n_1}}\\ &+\sum_{n_1}{}'\frac{\langle PaPb|I'(\Delta)|Qan_1\rangle\langle n_1|T_0|Qb\rangle}{\varepsilon_{Qb}-\varepsilon_{n_1}}\Bigg]\Bigg\}\,,\end{aligned} \tag{63}$$

$$\Delta E^{{\rm VP}(G3)}_{\rm SQED} = \langle Pa|U^{\rm el}_{\rm VP}|Pa\rangle\langle PaPb|I''(\Delta)|QaQb\rangle\Big(\langle Qb|T_0|Qb\rangle-\langle Pb|T_0|Pb\rangle\Big)\,, \tag{64}$$

$$\Delta E^{{\rm VP}(H)}_{\rm SQED} = \frac{1}{2}\,\langle PaPb|I'(\Delta)|QaQb\rangle\Big(\langle Qb|U^{\rm ml}_{\rm VP}|Qb\rangle-\langle Pb|U^{\rm ml}_{\rm VP}|Pb\rangle\Big)\,, \tag{65}$$

$$\Delta E^{{\rm VP}(I)}_{\rm SQED} = \frac{1}{2}\,\langle PaPb|I_{\rm VP}{}'(\Delta)|QaQb\rangle\Big(\langle Qb|T_0|Qb\rangle-\langle Pb|T_0|Pb\rangle\Big)\,. \tag{66}$$

The numerical calculations of the screened vacuum-polarization corrections are performed in coordinate space employing the finite basis set constructed from the DKB-splines [54]. For the electric-loop potential $U_{\rm VP}^{\rm el}$, that enters $\Delta E_{\rm SQED}^{{\rm VP}(A)}$, $\Delta E_{\rm SQED}^{{\rm VP}(B)}$, $\Delta E_{\rm SQED}^{{\rm VP}(E)}$, and $\Delta E_{\rm SQED}^{{\rm VP}(G)}$, we employ the well-known expression for the Uehling part and the approximate formulas from Ref. [59] for the Wichmann-Kroll part. The magnetic-loop potential $U_{\rm VP}^{\rm ml}$ ($\Delta E_{\rm SQED}^{{\rm VP}(C)}$ and $\Delta E_{\rm SQED}^{{\rm VP}(H)}$) is taken in the Uehling approximation only. In case of the g factor this leads to zero contribution. In case of the hyperfine structure we use the expression for the extended nucleus from Ref. [47]. For the operator $I_{\rm VP}$ ($\Delta E_{\rm SQED}^{{\rm VP}(F)}$ and $\Delta E_{\rm SQED}^{{\rm VP}(I)}$) we also employ the Uehling approximation, the corresponding expressions are taken from Ref. [58]. The calculational procedure has been checked utilizing the Feynman and Coulomb gauges for the photon propagator mediating the interelectronic interaction. The results in both gauges are presented term by term in Tables I and II for the g factor of $^{208}{\rm Pb}^{79+}$ and for the hyperfine splitting of $^{209}{\rm Bi}^{83+}$, respectively.

V. RESULTS AND DISCUSSION

A. *g* factor

The total value of the g factor of a Li-like ion can be written as

$$g = g_{\rm D} + \Delta g_{\rm int} + \Delta g_{\rm QED} + \Delta g_{\rm SQED} + \Delta g_{\rm nuc}\,. \tag{67}$$

Here $g_{\rm D}$ is the Dirac value, $\Delta g_{\rm int}$ is the interelectronic-interaction correction, $\Delta g_{\rm QED}$ is the one-electron QED correction, $\Delta g_{\rm SQED}$ is the screened QED correction, and $\Delta g_{\rm nuc}$ is the contribution of nuclear effects (finite nuclear size, nuclear recoil and nuclear polarization). To the first order in α and $1/Z$ the screened QED correction is defined by the set of the two-electron QED diagrams evaluated in the present paper. The operator T_0 in this case reads

$$T_0 = \mu_0\,[\mathbf{r}\times\boldsymbol{\alpha}]\cdot\boldsymbol{\mathcal{H}}\,, \tag{68}$$

where $\mu_0 = |e|/2$ is the Bohr magneton, $\boldsymbol{\mathcal{H}}$ is the magnetic field directed along the z-axis. The corresponding contribution to the g factor is given by

$$\Delta g_{\rm SQED} = \Delta g_{\rm SQED}^{\rm SE} + \Delta g_{\rm SQED}^{\rm VP}\,, \tag{69}$$

$$\Delta g_{\rm SQED}^{\rm SE/VP} = \Delta E_{\rm SQED}^{\rm SE/VP}/(\mu_0 \mathcal{H} m_j)\,, \tag{70}$$

where m_j is the z-projection of the total angular momentum. In Table I the contributions of the individual terms to $\Delta g^{\rm SE}_{\rm SQED}$ and $\Delta g^{\rm VP}_{\rm SQED}$ are presented in the Feynman and Coulomb gauges. The contributions of $\Delta E^{{\rm VP}(C)}_{\rm SQED}$ and $\Delta E^{{\rm VP}(H)}_{\rm SQED}$ are zero in the Uehling approximation that we employed for $U^{\rm ml}_{\rm VP}$. The diagram F, which is gauge invariant itself, is calculated only in the Feynman gauge. It can be seen from the table that the total results in the different gauges are in a fair agreement with each other. Additionally, we estimated the Wichmann-Kroll part of the magnetic-loop diagrams taking the one-electron value from Ref. [15], and assuming the same screening ratio as for the electric-loop diagrams.

In Table III the individual terms and the total values of the g factor for Li-like lead $^{208}{\rm Pb}^{79+}$ and uranium $^{238}{\rm U}^{89+}$ are presented. The contribution of the screened self-energy correction $\Delta g^{\rm SE}_{\rm SQED}$ amounts to $-3.3(2)\times10^{-6}$ for $^{208}{\rm Pb}^{79+}$ and $-4.9(9)\times10^{-6}$ for $^{238}{\rm U}^{89+}$. The estimated uncertainty of the result is rather large due to the cancellation of the individual terms presented in Table I. The values obtained previously with local screening potentials are $-3.5(1.2)\times10^{-6}$ and $-3.1(1.5)\times10^{-6}$, respectively [27]. The contribution of the screened vacuum-polarization $\Delta g^{\rm VP}_{\rm SQED}$ is $1.53(3)\times10^{-6}$ for $^{208}{\rm Pb}^{79+}$ and $2.55(5)\times10^{-6}$ for $^{238}{\rm U}^{89+}$. The other contributions to the g factor presented in Table III were considered in details in our previous studies [26, 27]. The accuracy of the g factor value is about 10% better than that from Ref. [27] and is almost completely determined by the higher-orders of the interelectronic-interaction correction.

B. Hyperfine splitting

The total value of the hyperfine splitting of a Li-like ion can be written as,

$$\Delta E^{(a)}_{\rm hfs} = E_F\left[A(\alpha Z)(1-\delta)(1-\varepsilon)+\frac{1}{Z}B(\alpha Z)+\frac{1}{Z^2}C(Z,\alpha Z)+x_{\rm QED}+x_{\rm SQED}\right]\,, \quad (71)$$

where E_F is the non-relativistic value of the hyperfine splitting (Fermi energy), $A(\alpha Z)$ is the one-electron relativistic factor, δ and ε are the corrections for distributions of the charge and magnetic moment over the nucleus, respectively. The interelectronic-interaction corrections of first and higher orders in $1/Z$ are represented by the functions $B(\alpha Z)$ and $C(Z,\alpha Z)$, respectively. The term $x_{\rm QED}$ corresponds to the one-electron QED corrections. The details on these contributions can be found in Refs. [40, 47] and references therein. The operator T_0 for the hyperfine splitting is given by

$$T_0 = E_F G_a \frac{[\mathbf{r}\times\boldsymbol{\alpha}]_z}{r^3}\,. \quad (72)$$

The factor G_a is defined by the quantum numbers of the valence state,

$$G_a = \frac{n^3(2l+1)j(j+1)}{2(\alpha Z)^3 m_j}\,, \tag{73}$$

where n is the principal quantum number, j and m_j are the angular momentum and its projection, and l defines the parity of the state. We note that T_0 is the effective one-particle operator, which is employed in calculations of various contributions to the hyperfine splitting. The full Hamiltonian of the hyperfine interaction is the well-known Fermi-Breit operator.

To the first order in α and $1/Z$ the screened QED correction $x_{\rm SQED}$ to the hyperfine splitting is given by

$$x_{\rm SQED} = x^{\rm SE}_{\rm SQED} + x^{\rm VP}_{\rm SQED}\,, \tag{74}$$

$$x^{\rm SE/VP}_{\rm SQED} = \Delta E^{\rm SE/VP}_{\rm SQED}/E_F\,. \tag{75}$$

In Table IV the screened self-energy and vacuum-polarization corrections to the hyperfine splitting are presented for several values of Z in the range $Z = 20$ – 83. The calculations are performed with the Fermi model for the finite nuclear charge distribution. The finite nuclear magnetization distribution is introduced via an additional factor $F(r)$ in the operator T_0 [47]. The individual contributions to $x^{\rm SE}_{\rm SQED}$ and $x^{\rm VP}_{\rm SQED}$ for lithiumlike bismuth $^{209}{\rm Bi}^{80+}$ are presented in Table II in the Feynman and Coulomb gauges. Perfect agreement is found between the total results in the different gauges. This is also true for the other values of Z. We mention, however that the contribution of the screened vacuum-polarization diagram F, which is gauge invariant itself, is calculated in the Feynman gauge only. For the screened Wichmann-Kroll magnetic-loop part we have employed the hydrogenic $2s$ value from Ref. [57], assuming that it enters with the same screening ratio as the Uehling terms.

In Table V we present the total value of the hyperfine splitting in bismuth in terms of the specific difference of the ground state hyperfine splitting in the H-like ion ($1s$) and in the Li-like ion ($2s$): $\Delta' E = \Delta E^{(2s)} - \xi \Delta E^{(1s)}$. It was proposed in Ref. [40] to consider this difference in order to overcome the problem of a large uncertainty of the Bohr-Weisskopf (BW) effect, originating from the nuclear magnetization distribution. The parameter ξ is chosen to cancel the BW correction, and the accuracy of the specific difference $\Delta' E$ appears to be much higher than the accuracy of the splittings $\Delta E^{(1s)}$ and $\Delta E^{(2s)}$ themselves. The value of $\xi = 0.16886$ has been found for bismuth, taking into account the BW effect on all of the contributions, presented in Table V. For the related discussion we refer to our Letter [48]. We only mention here that the rms radius was taken to

be $\langle r^2\rangle^{1/2} = 5.5211$ fm [60], the nuclear spin and parity $I^\pi = 9/2-$, and the magnetic moment $\mu = 4.1106(2)\mu_N$ [61].

C. Conclusion

The rigorous evaluation of the screened QED corrections to the g factor and to the hyperfine splitting of heavy Li-like ions within *ab initio* QED approach has been performed. Previously developed procedures for the evaluation of the one-electron QED corrections in presence of the external magnetic field and of the two-electron QED corrections to the energy levels have been associated and generalized. The complete gauge-invariant set of the two-electron self-energy diagrams with external magnetic field has been calculated. The dominant part of the two-electron vacuum-polarization correction has been calculated as well. The electric-loop diagrams have been evaluated for both Uehling and Wichmann-Kroll parts. The magnetic-loop diagrams have been evaluated in the Uehling approximation. These results improve the accuracy of the theoretical predictions for the g factor and the hyperfine splitting of heavy ions where stringent tests of the bound-state QED effects are feasible.

Acknowledgments

Valuable conversations with A. N. Artemyev are gratefully acknowledged. This work was supported by RFBR (Grant No. 07-02-00126-a), GSI, DFG (Grant No. 436RUS113/950/0-1), and by the Ministry of Education and Science of Russian Federation (Program for Development of Scientific Potential of High School, Grant No. 2.1.1/1136; Program Scientific and pedagogical specialists for innovative Russia) and by the grant of the President of Russian Federation. D.A.G. acknowledges the support by the FAIR – Russia Research Center, and by Saint-Petersburg Government. V.M.S. acknowledges the support by the Alexander von Humboldt Foundation.

[1] N. Hermanspahn, H. Häffner, H.-J. Kluge, W. Quint, S. Stahl, J. Verdú, and G. Werth, Phys. Rev. Lett. **84**, 427 (2000).

[2] H. Häffner, T. Beier, N. Hermanspahn, H.-J. Kluge, W. Quint, S. Stahl, J. Verdú, and G. Werth, Phys. Rev. Lett. **85**, 5308 (2000).

[3] J. L. Verdú, S. Djekic, S. Stahl, T. Valenzuela, M. Vogel, G. Werth, T. Beier, H.-J. Kluge, and W. Quint, Phys. Rev. Lett. **92**, 093002 (2004).

[4] P. J. Mohr, B. N. Taylor, and D. B. Newell, Rev. Mod. Phys. **80**, 633 (2008).

[5] M. Vogel, J. Alonso, K. Blaum, W. Quint, B. Schabinger, S. Sturm, J. Verdú, A. Wagner, and G. Werth, Eur. Phys. J. Special Topics **163**, 113 (2008).

[6] H.-J. Kluge, T. Beier, K. Blaum, L. Dahl, S. Eliseev, F. Herfurth, B. Hofmann, O. Kester, S. Koszudowski, C. Kozhuharov, G. Maero, W. Nörtershäuser, J. Pfister, W. Quint, U. Ratzinger, A. Schempp, R. Schuch, T. Stöhlker, R. C. Thompson, M. Vogel, G. Vorobjev, D. F. A. Winters and G. Werth, Adv. Quantum Chem. **53**, 83 (2008).

[7] M. Vogel and W. Quint, J. Phys. B **42**, 154016 (2009).

[8] V. M. Shabaev, D. A. Glazov, N. S. Oreshkina, A. V. Volotka, G. Plunien, H.-J. Kluge, and W. Quint, Phys. Rev. Lett. **96**, 253002 (2006).

[9] S. A. Blundell, K. T. Cheng, and J. Sapirstein, Phys. Rev. A **55**, 1857 (1997).

[10] H. Persson, S. Salomonson, P. Sunnergren, and I. Lindgren, Phys. Rev. A **56**, R2499 (1997).

[11] T. Beier, I. Lindgren, H. Persson, S. Salomonson, P. Sunnergren, H. Häffner, and N. Hermanspahn, Phys. Rev. A **62**, 032510 (2000).

[12] S. G. Karshenboim, V. G. Ivanov, and V. M. Shabaev, Can. J. Phys. **79**, 81 (2001); Zh. Eksp. Teor. Fiz. **120**, 546 (2001) [Sov. Phys. JETP **93**, 477 (2001)].

[13] S. G. Karshenboim and A. I. Milstein, Phys. Lett. B **549**, 321 (2002).

[14] V. A. Yerokhin, P. Indelicato, and V. M. Shabaev, Phys. Rev. Lett. **89**, 143001 (2002); Phys. Rev. A **69**, 052503 (2004).

[15] R. N. Lee, A. I. Milstein, I. S. Terekhov, and S. G. Karshenboim, Phys. Rev. A **71**, 052501 (2005).

[16] V. A. Yerokhin and U. D. Jentschura, Phys. Rev. Lett. **100**, 163001 (2008); Phys. Rev. A **81**, 012502 (2010).

[17] K. Pachucki, A. Czarnecki, U. D. Jentschura, and V. A. Yerokhin, Phys. Rev. A **72**, 022108 (2005).

[18] U. D. Jentschura, Phys. Rev. A **79**, 044501 (2009).

[19] V. M. Shabaev, Phys. Rev. A **64**, 052104 (2001).

[20] V. M. Shabaev and V. A. Yerokhin, Phys. Rev. Lett. **88**, 091801 (2002).

[21] K. Pachucki, Phys. Rev. A **78**, 012504 (2008).

[22] A. V. Nefiodov, G. Plunien, and G. Soff, Phys. Rev. Lett. **89**, 081802 (2002).

[23] D. A. Glazov and V. M. Shabaev, Phys. Lett. A **297**, 408 (2002).

[24] Z.-C. Yan, J. Phys. B **35**, 1885 (2002).

[25] V. M. Shabaev, D. A. Glazov, M. B. Shabaeva, V. A. Yerokhin, G. Plunien, and G. Soff, Phys. Rev. A **65**, 062104 (2002).

[26] D. A. Glazov, V. M. Shabaev, I. I. Tupitsyn, A. V. Volotka, V. A. Yerokhin, G. Plunien, and G. Soff, Phys. Rev. A **70**, 062104 (2004).

[27] D. A. Glazov, A. V. Volotka, V. M. Shabaev, I. I. Tupitsyn, and G. Plunien, Phys. Lett. A **357**, 330 (2006).

[28] I. Klaft, S. Borneis, T. Engel, B. Fricke, R. Grieser, G. Huber, T. Kühl, D. Marx, R. Neumann, S. Schröder, P. Seelig, and L. Völker, Phys. Rev. Lett. **73**, 2425 (1994).

[29] J. R. Crespo López-Urrutia, P. Beiersdorfer, D. W. Savin, and K. Widmann, Phys. Rev. Lett. **77**, 826 (1996).

[30] J. R. Crespo López-Urrutia, P. Beiersdorfer, K. Widmann, B. B. Birkett, A.-M. Mårtensson-Pendrill, and M. G. H. Gustavsson, Phys. Rev. A **57**, 879 (1998).

[31] P. Seelig, S. Borneis, A. Dax, T. Engel, S. Faber, M. Gerlach, C. Holbrow, G. Huber, T. Kühl, D. Marx, K. Meier, P. Merz, W. Quint, F. Schmitt, M. Tomaselli, L. Völker, H. Winter, M. Würtz, K. Beckert, B. Franzke, F. Nolden, H. Reich, M. Steck, and T. Winkler, Phys. Rev. Lett. **81**, 4824 (1998).

[32] P. Beiersdorfer, S. B. Utter, K. L. Wong, J. R. Crespo López-Urrutia, J. A. Britten, H. Chen, C. L. Harris, R. S. Thoe, D. B. Thorn, E. Trabert, M. G. H. Gustavsson, C. Forssén, and A.-M. Mårtensson-Pendrill, Phys. Rev. A **64**, 032506 (2001).

[33] H. Persson, S. M. Schneider, W. Greiner, G. Soff, and I. Lindgren, Phys. Rev. Lett. **76**, 1433 (1996).

[34] S. A. Blundell, K. T. Cheng, and J. Sapirstein, Phys. Rev. Lett. **78**, 4914 (1997).

[35] V. M. Shabaev, M. Tomaselli, T. Kühl, A. N. Artemyev, and V. A. Yerokhin, Phys. Rev. A **56**, 252 (1997).

[36] P. Sunnergren, H. Persson, S. Salomonson, S. M. Schneider, I. Lindgren, and G. Soff, Phys. Rev. A **58**, 1055 (1998).

[37] S. Boucard and P. Indelicato, Eur. Phys. J. D **8**, 59 (2000).

[38] V. M. Shabaev, A. N. Artemyev, O. M. Zherebtsov, V. A. Yerokhin, G. Plunien, and G. Soff, Hyp. Int. **27**, 279 (2000).

[39] J. Sapirstein and K. T. Cheng, Phys. Rev. A **63**, 032506 (2001).

[40] V. M. Shabaev, A. N. Artemyev, V. A. Yerokhin, O. M. Zherebtsov, and G. Soff, Phys. Rev. Lett. **86**, 3959 (2001).

[41] P. Beiersdorfer, A. L. Osterheld, J. H. Scofield, J. R. Crespo López-Urrutia, and K. Widmann, Phys. Rev. Lett. **80**, 3022 (1998).

[42] D. F. A. Winters, M. Vogel, D. M. Segal, R. C. Thompson, and W. Nörtershäuser, Can. J. Phys. **85**, 403 (2007).

[43] J. Sapirstein and K. T. Cheng, Phys. Rev. A **67**, 022512 (2003); Phys. Rev. A **74**, 042513 (2006); Phys. Rev. A **78**, 022515 (2008).

[44] N. S. Oreshkina, A. V. Volotka, D. A. Glazov, I. I. Tupitsyn, V. M. Shabaev, and G. Plunien, Opt. Spektrosk. **102**, 889 (2007) [Opt. Spectrosc. **102**, 815 (2007)].

[45] Y. S. Kozhedub, D. A. Glazov, A. N. Artemyev, N. S. Oreshkina, V. M. Shabaev, I. I. Tupitsyn, A. V. Volotka, and G. Plunien, Phys. Rev. A **76**, 012511 (2007).

[46] N. S. Oreshkina, D. A. Glazov, A. V. Volotka, V. M. Shabaev, I. I. Tupitsyn, and G. Plunien, Phys. Lett. A **372**, 675 (2008).

[47] A. V. Volotka, D. A. Glazov, I. I. Tupitsyn, N. S. Oreshkina, G. Plunien, and V. M. Shabaev, Phys. Rev. A **78**, 062507 (2008).

[48] A. V. Volotka, D. A. Glazov, V. M. Shabaev, I. I. Tupitsyn, and G. Plunien, Phys. Rev. Lett. **103**, 033005 (2009).

[49] V. M. Shabaev, Phys. Rep. **356**, 119 (2002).

[50] N. J. Snyderman, Ann. Phys. (N.Y.) **211**, 43 (1991).

[51] S. A. Blundell and N. J. Snyderman, Phys. Rev. A **44**, R1427 (1991).

[52] V. A. Yerokhin and V. M. Shabaev, Phys. Rev. A **60**, 800 (1999).

[53] V. A. Yerokhin, A. N. Artemyev, T. Beier, G. Plunien, V. M. Shabaev, and G. Soff, Phys. Rev. A **60**, 3522 (1999).

[54] V. M. Shabaev, I. I. Tupitsyn, V. A. Yerokhin, G. Plunien, and G. Soff, Phys. Rev. Lett. **93**, 130405 (2004).

[55] J. Sapirstein and W. R. Johnson, J. Phys. B **29**, 5213 (1996).

[56] P. J. Mohr, G. Plunien, and G. Soff, Phys. Rep. **293**, 227 (1998).

[57] A. N. Artemyev, V. M. Shabaev, G. Plunien, G. Soff, and V. A. Yerokhin, Phys. Rev. A **63**, 062504 (2001).

[58] A. N. Artemyev, T. Beier, G. Plunien, V. M. Shabaev, G. Soff, and V. A. Yerokhin, Phys. Rev. A **60**, 45 (1999).

[59] A. G. Fainshtein, N. L. Manakov, and A. A. Nekipelov, J. Phys. B **23**, 559 (1990).

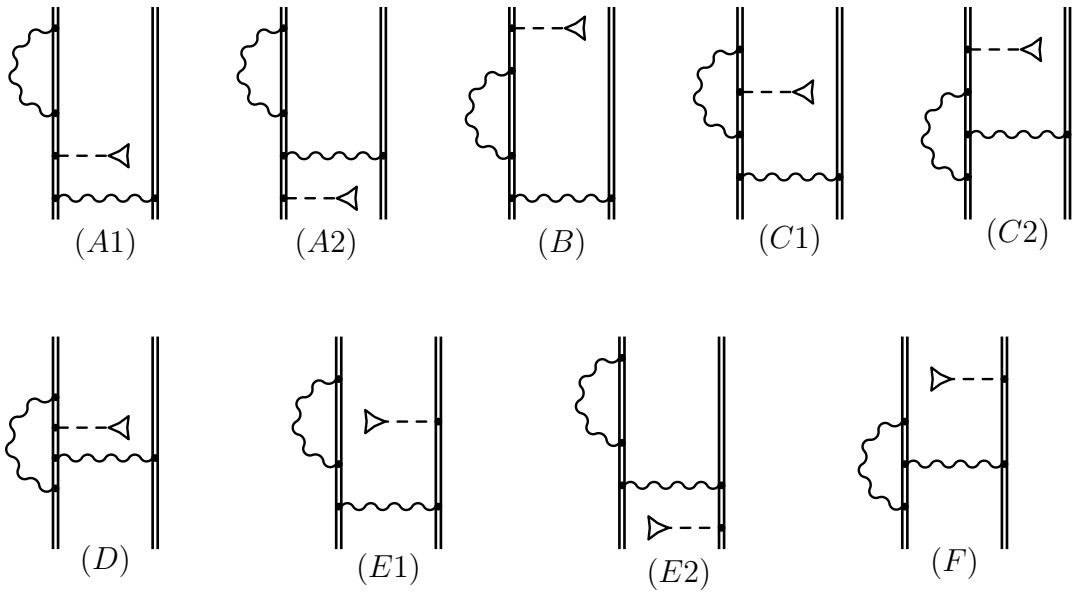

FIG. 1: Feynman diagrams representing the screened self-energy correction in the presence of an external magnetic field. The wavy line indicates the photon propagator and the double line indicates the electron propagators in the Coulomb field. The dashed line terminated with the triangle denotes the interaction with the magnetic field.

[60] I. Angeli, At. Data Nucl. Data Tables **87**, 185 (2004).

[61] N. J. Stone, At. Data Nucl. Data Tables **90**, 75 (2005).

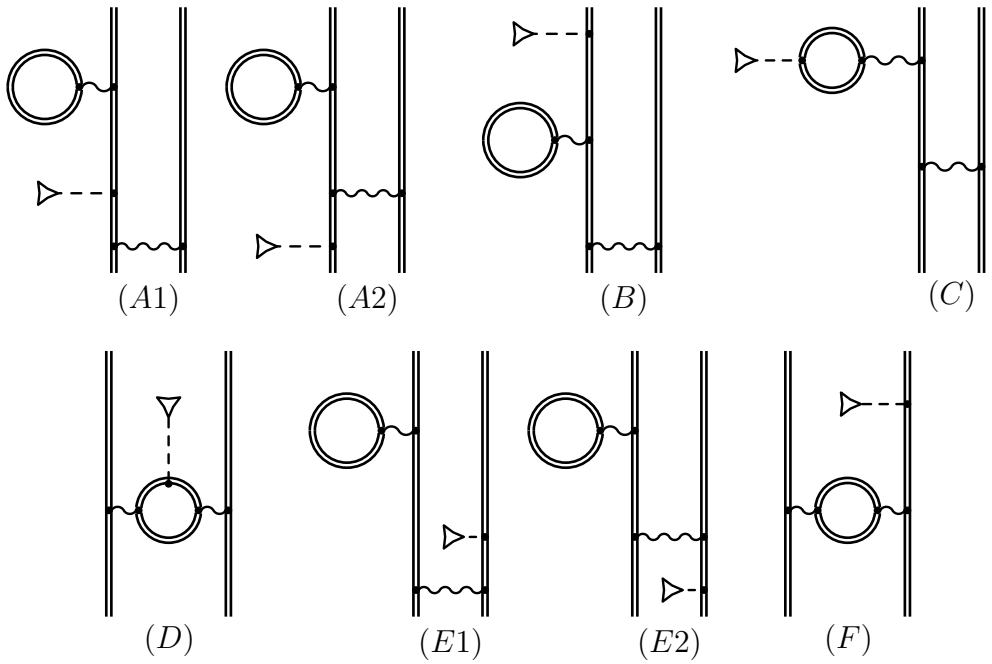

FIG. 2: Feynman diagrams representing the screened vacuum-polarization correction in the presence of an external magnetic field. The notations are the same as in Fig. 1.

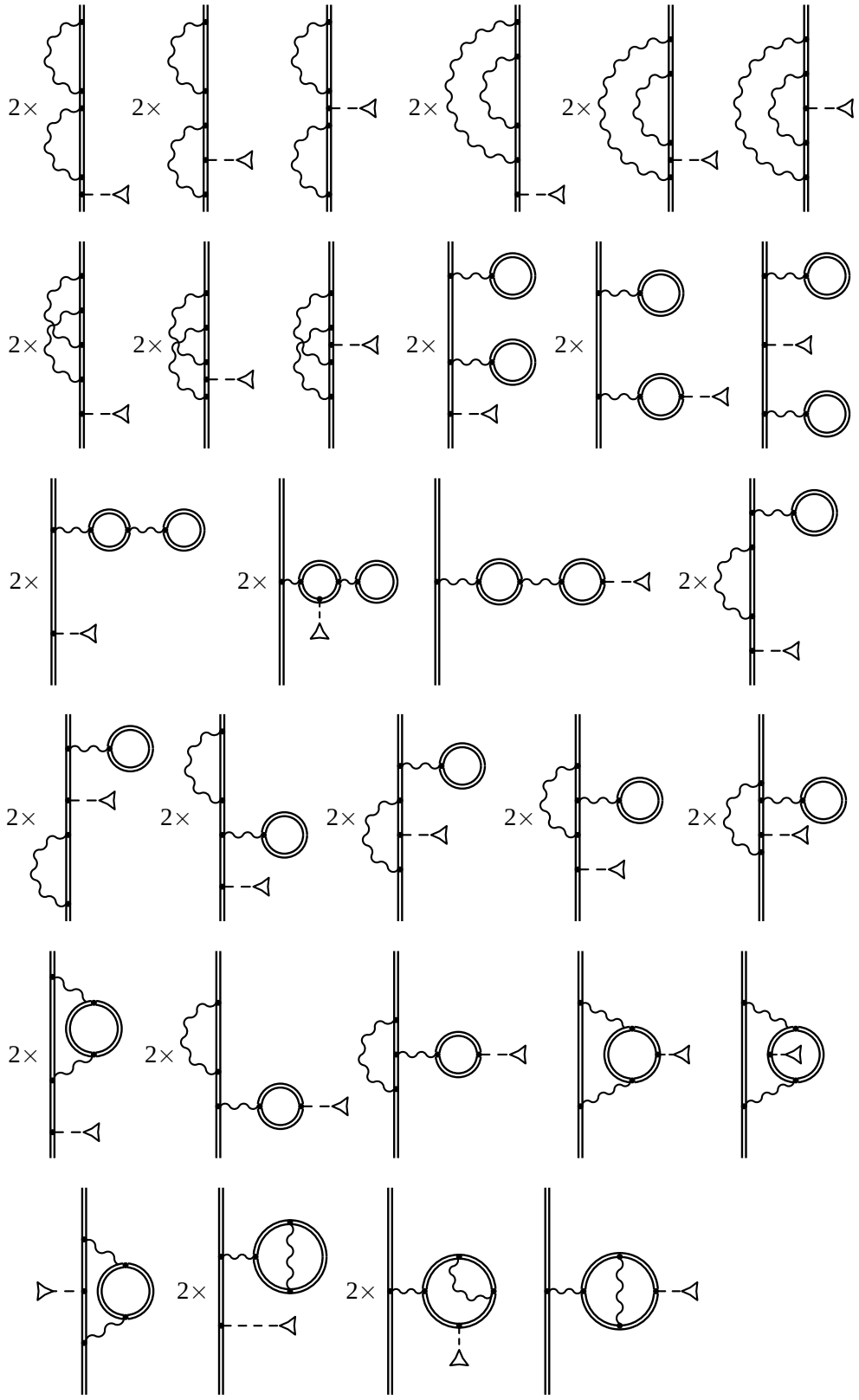

FIG. 3: Feynman diagrams representing the two-loop QED corrections in the presence of an external potential. The notations are the same as in Fig. 1.

TABLE I: Contributions of the individual terms to the screened self-energy and vacuum-polarization corrections to the g factor of Li-like lead $^{208}\mathrm{Pb}^{79+}$. The units are 10^{-6}.

	Screened SE			Screened VP	
	Feynman	Coulomb		Feynman	Coulomb
A	171.7	173.6	A	−34.27	−34.65
B	18.1	18.5	B	0.83	0.82
C	−30.5	−31.6	C	—	—
D	−52.3	−52.0	D	—	—
E	−1.0	−1.0	E	0.16	0.15
F	4.2	4.2	F	−0.01	—
G	−167.3	−169.2	G	34.89	35.29
H	−41.3	−41.3	H	—	—
I	95.3	95.5	I	0.00	—
Total SE	−3.3	−3.3	Total(A-I)	1.60	1.60
			WK-ml	−0.06(3)	
			Total VP	1.54(3)	

TABLE II: Contributions of the individual terms to the screened self-energy and vacuum-polarization corrections to the hyperfine splitting of Li-like bismuth $^{209}\mathrm{Bi}^{80+}$ in terms of x_{SQED}.

	Screened SE			Screened VP	
	Feynman	Coulomb		Feynman	Coulomb
A	0.001544	0.001555	A	−0.0004881	−0.0004892
B	−0.000380	−0.000398	B	−0.0002128	−0.0002103
C	0.001928	0.001952	C	−0.0001691	−0.0001669
D	−0.000936	−0.000945	D	—	—
E	0.000028	0.000028	E	−0.0000031	−0.0000029
F	−0.000174	−0.000172	F	0.0000015	—
G	−0.001298	−0.001307	G	0.0002766	0.0002749
H	0.000331	0.000331	H	0.0000023	0.0000001
I	0.000066	0.000066	I	0.0000000	—
Total SE	0.001109	0.001109	Total(A-I)	−0.0005927	−0.0005927
			WK-ml	0.00005(2)	
			Total VP	−0.00054(2)	

TABLE III: Individual contributions to the ground-state g factor of Li-like lead $^{208}\mathrm{Pb}^{79+}$ and uranium $^{238}\mathrm{U}^{89+}$.

	$^{208}\mathrm{Pb}^{79+}$	$^{238}\mathrm{U}^{89+}$
Dirac value (point nucleus)	1.932 002 904	1.910 722 624 (1)
Finite nuclear size	0.000 078 58 (13)	0.000 241 30 (43)
Interelectronic interaction, $\sim 1/Z$	0.002 148 29	0.002 509 84
Interelectronic interaction, $\sim 1/Z^2$ and h.o.	−0.000 007 6 (27)	−0.000 008 5 (38)
QED, $\sim \alpha$	0.002 411 7 (1)	0.002 446 3 (2)
QED, $\sim \alpha^2$	−0.000 003 6 (5)	−0.000 003 6 (8)
Screened SE	−0.000 003 3 (2)	−0.000 004 9 (9)
Screened VP	0.000 001 54 (3)	0.000 002 55 (5)
Nuclear recoil	0.000 000 25 (35)	0.000 000 28 (69)
Nuclear polarization	−0.000 000 04 (2)	−0.000 000 27 (14)
Total	1.936 628 7 (28)	1.915 905 7 (41)

TABLE IV: Screened QED corrections to the hyperfine splitting of lithiumlike ions.

Z	$x^{\mathrm{SE}}_{\mathrm{SQED}}$	$x^{\mathrm{VP}}_{\mathrm{SQED}}$	x_{SQED}
20	0.000256	−0.000116	0.000140(1)
30	0.000330	−0.000131	0.000199(1)
40	0.000394	−0.000155	0.000238(1)
50	0.000473	−0.000186(3)	0.000287(3)
60	0.000582	−0.000241(4)	0.000340(4)
70	0.00075	−0.00033(1)	0.00042(1)
83	0.00111	−0.00054(2)	0.00057(2)

TABLE V: Individual contributions to the specific difference $\Delta' E$ of the hyperfine splittings for bismuth ^{209}Bi. The units are meV.

	$\Delta E^{(2s)}$	$\xi \Delta E^{(1s)}$	$\Delta' E$
Dirac value	844.829	876.638	−31.809
Interelectronic interaction, $\sim 1/Z$	−29.995		−29.995
Interelectronic interaction, $\sim 1/Z^2$ and h.o.	0.25(4)		0.25(4)
QED	− 5.052	−5.088	0.036
Screened SE	0.381		0.381
Screened VP	− 0.187(6)		− 0.187(6)
Total			−61.32(4)